IEEE Access
Multidisciplinary | Rapid Review | Open Access Journal

Date of publication xxxx 00, 0000, date of current version xxxx 00, 0000.

Digital Object Identifier 10.1109/ACCESS.2019.Doi Number

Fuzzy Dynamic Thermal Rating System based SIPS for Enhancing Transmission Line Security

MOHAMED K. METWALY[1] AND JIASHEN TEH[3], (Member, IEEE)

[1]Electrical Engineering Department, Faculty of Engineering, Taif University, Taif 21974, Kingdom of Saudi Arabia.

[2]School of Electrical and Electronic Engineering, Engineering Campus, Universiti Sains Malaysia (USM), Nibong Tebal, Penang 14300, Malaysia

Corresponding author: Jiashen Teh (e-mail: jiashenteh@usm.my)

The authors extend their appreciation to the Deputyship for Research & Innovation, Ministry of Education, Saudi Arabia, for funding this research work through the project number 284.

ABSTRACT The increased integrations of intermittent renewable energy sources into power systems cause more power grid congestions and therefore system operators need more advanced control to relieve this pressure. The dynamic thermal rating (DTR) system is able to increase the thermal constraint and subsequently maximum loading of existing lines. This dynamic rating is achieved through real-time considerations of weather data and it is usually much higher than the traditional static thermal rating system. The operational tripping scheme (OTS), a variant of the wider system integrity protection scheme, also relieves line congestions but it does this by tripping pre-selected generators and this have the unwanted consequence of reducing power adequacy. This paper proposes the novel integration of DTR and OTS, while considering the inherent uncertainties of their sensors based on fuzzy numbers, to avoid unnecessary generation tripping due to conservative line ratings. This novel Fuzzy-DTR-OTS delays the tripping of generations, enhances the adequacy of power supply, improves system security and avoids high risk cascading black out inducing events.

INDEX TERMS dynamic thermal rating, SIPS, conductor temperature, wide area monitoring

NOMENCLATURE

Constants

mc_p	Conductor heat capacity (J/m · ℃)
ρ_f	Density of air (kg/m^3)
H_e	Conductor elevation above sea level (m)
D	Conductor diameter (m)
ε	Emissivity of conductor (0.23 to 0.91)
Lat	Degrees of latitude in degrees
Z_l	Azimuth of line in degrees
ψ	Solar absorptivity (0.23 to 0.91)
Ar	Projected area of conductor to the sun (m^2/m)
δ	Solar declination in degrees (0° to 90°)
T_H, T_L	Maximum and minimum conductor temperature (℃)
$R(T_L)$, $R(T_H)$	AC conductor resistance at T_L and T_H, respectively (Ω/m)
C	Solar azimuth constant in degrees

Fuzzy number

A^α	α-cut of fuzzy number A
A_1^α, A_2^α	Lower and upper limits of fuzzy number A
$\mu_A(x)$	Membership function of fuzzy number A

Measured variables

I	(crisp value)	Line current (A)
I_i	(crisp value)	Initial line current (A)
I_f	(crisp value)	Final line current (A)
$V_w : V_w^\alpha = [V_{w1}^\alpha, V_{w2}^\alpha]$		Wind speed (m/s)
$T_a : T_a^\alpha = [T_{a1}^\alpha, T_{a2}^\alpha]$		Ambient air temperature (℃)
$\varphi : \varphi^\alpha = [\varphi_1^\alpha, \varphi_2^\alpha]$		Wind angle in degrees
$\omega : \omega^\alpha = [\omega_1^\alpha, \omega_2^\alpha]$		Solar hour angle in degrees

Calculated variables

T_{film}^α	$= \begin{bmatrix} T_{film1}^\alpha, \\ T_{film2}^\alpha \end{bmatrix}$	Average of conductor and ambient temperature (℃)
ρ_f^α	$= [\rho_{f1}^\alpha, \rho_{f2}^\alpha]$	Density of air (kg/m^3)
μ_f^α	$= [\mu_{f1}^\alpha, \mu_{f2}^\alpha]$	Dynamic air viscosity (Pa · s)
k_f^α	$= [k_{f1}^\alpha, k_{f2}^\alpha]$	Thermal conductivity of air (W/ m · ℃)
k_{angle}^α	$= \begin{bmatrix} k_{angle1}^\alpha, \\ k_{angle2}^\alpha \end{bmatrix}$	Wind director factor

This article has been accepted for publication in a future issue of this journal, but has not been fully edited. Content may change prior to final publication. Citation information: DOI 10.1109/ACCESS.2021.3086866, IEEE Access

Q_c^α	$= [Q_{c1}^\alpha, Q_{c2}^\alpha]$	Convection heat loss (W/m^2)
Q_r^α	$= [Q_{r1}^\alpha, Q_{r2}^\alpha]$	Radiation heat loss (W/m^2)
H_c^α	$= [H_{c1}^\alpha, H_{c2}^\alpha]$	Altitude of sun in degrees
Q_{se}^α	$= \begin{bmatrix} Q_{se1}^\alpha, \\ Q_{se2}^\alpha \end{bmatrix}$	Radiation heat gain at elevation corrected (W/m^2)
q_s^α	$= [q_{s1}^\alpha, q_{s2}^\alpha]$	Heat gain rate from sun (W/m)
Z_c^α	$= [Z_{c1}^\alpha, Z_{c2}^\alpha]$	Azimuth of sun in degrees
χ^α	$= [\chi_1^\alpha, \chi_2^\alpha]$	Solar azimuth variable
θ^α	$= [\theta_1^\alpha, \theta_2^\alpha]$	Incidence sun angle in degrees
Q_s^α	$= [Q_{s1}^\alpha, Q_{s2}^\alpha]$	Radiation heat gain (W/m^2)
T_c^α	$= [T_{c1}^\alpha, T_{c2}^\alpha]$	Conductor temperature (°C)
T_i^α	$= [T_{i1}^\alpha, T_{i2}^\alpha]$	Initial conductor temperature (°C)
T_f^α	$= [T_{f1}^\alpha, T_{f2}^\alpha]$	Final conductor temperature (°C)
$T_{c,s1}^\alpha, T_{c,s2}^\alpha, \dots, T_{c,sN}^\alpha$		Conductor temperatures at span 1, 2, …, N (°C)

I. INTRODUCTION

The growing demand of electricity and awareness for cutting CO2 emissions to curb global temperature rise has drastically increased the integrations of intermittent renewable energy sources such as wind [1]–[4] and solar [5]–[8], energy storage systems to support renewables [9]–[11], demand response to actively manage load profiles [12]–[17], electric vehicles, FACTS devices for voltage and reactive power regulations and HVDC transmission corridors for long distance power transfer. Due to this, the operation limits of power grids have been pushed further than ever before. Consequently, modern power systems have become more complex and challenging to operate, which is due to higher number of faults on transmission networks, operations that are closer to security limits, and higher emphasis of reliability, economic and environmental factors that are all difficult to optimize together [18].

In view of these challenges and uncertainties, there is a need for effective plans that can restore grid integrity to normal conditions as fast and as closely as possible with reasonable cost during contingencies, and the system integrity protection scheme (SIPS) fits this set of criteria [19]. Conventionally, power protection systems are designed to detect, mitigate and isolate faults of power system components by comparing certain conditions, i.e., overcurrent and voltage, against specific thresholds, which are determined based on conservative assumptions of operating conditions. Despite being a reliable protection scheme, this conventional method suppresses the actual capacity of grids and does not take advantage of recent advancement in information and communication technologies that have enable wide area monitoring (WAM), causing a lapse in informed decision making [20]–[22]. Instead of triggering protection systems based on fixed thresholds, SIPS dynamically adjusts the thresholds in real-time according to critical grid conditions that are monitored through various sensors. Under SIPS, the efficiency and security of various power protection schemes, i.e., generation rejection, overload mitigation and etc., are now highly reliable and has been accepted worldwide [23]. In the Saudi Arabia (SA) national grid, a variant of SIPS, the Operational Tripping Scheme (OTS), was installed in a special pilot zone of the grid to study the efficacy of OTS in tripping power generations after the loss of transmission lines to protect against line overloading and cascading outages [24].

Given that line overloading is determined based on conductor temperatures (proportional to line rating) [25], and that the dynamic thermal rating (DTR) system of overhead transmission lines can provide actual calculations of conductor temperatures based on the IEEE 738 standard [26], the integration of DTR and OTS, known as DTR-OTS, are examined in detailed in this paper. Unlike the static thermal rating (STR) system which applies a set of very conservative weather assumptions onto the calculation of line ratings/temperatures, the DTR system uses real-time weather conditions. As studies have shown that actual weather conditions are most of the time overwhelmingly more desirable than the assumptions made in the STR system, the approach of the DTR system provides huge potential rating upsides [27]–[30].

Therefore, the key benefit of deploying the DTR-OTS system is an improved understanding of conductor temperatures, and this new found information can be capitalized to optimally trip generations at the right time, to maximize line loadings and power deliveries, and to provide greater situational awareness to system operators [31]. Similar benefit on the protection of switchgear and transformer has also been demonstrated before [32]. Through the DTR, the OTS can accurately identify whether thermal overloads will happen after the occurrence of contingencies, i.e., line losses, and exactly when conductor thermal limit will be exceeded in the future if overloading takes place, without resorting to assumptions. Compared to the STR based OTS (STR-OTS), which at best can only assume that thermal overload will happen at some unknown time in the future, the situational awareness provided by the DTR-OTS offers significant values. Knowing the time of exceedance of conductor temperature enables system operators to replace costly and intrusive generation tripping with optimal power re-dispatch that may delay power tripping or avoid it altogether.

At the same time, a great deal of uncertainty exists in the measurements of weather data used for DTR calculations, which could stem from inherent measurement errors, insufficient sampling points along transmission lines, and unpredictable changes of weather conditions. Therefore, in order to achieve realistic DTR calculations, these uncertainties should be considered. Although probabilistic technique is often used to model uncertainties, it requires specific probability distributions (and their parameters) to be assigned to the uncertain parameters, and this is only possible

This article has been accepted for publication in a future issue of this journal, but has not been fully edited. Content may change prior to final publication. Citation information: DOI 10.1109/ACCESS.2021.3086866, IEEE Access

with sufficient historical records to form a reliable statistical inference, which is not always available [33]. Instead, the fuzzy set has been identified to be more appropriate in modelling uncertainty of weather data [34], [35]. Moreover, fuzzy reasoning has also been successfully used to optimally control transmission line overloading [36], and fuzzy based control system has also been proposed to calculate line ratings [37]. Due to the above, the fuzzy model is also proposed for DTR calculations in the earlier proposed DTR-OTS system to accommodate the uncertainties associated with weather data.

The two novelties of this paper is as follows: (1) the integration of DTR and OTS, known as DTR-OTS, to optimize the timing of generation tripping. The DTR system is better than the STR system in the sense that higher line capacity can be achieved, allowing higher loading and delay OTS tripping. Moreover, the time-delay response of conductor temperature allows more time for tripping action to be taken instead of instantaneous. (2) the used of fuzzy set in DTR calculations, known as Fuzzy-DTR-OTS (FDTR-OTS), to accommodate weather data uncertainty, which is performed for the first time in OTS modelling.

The general principles of OTS and descriptions of SA national grid OTS are presented in section II. In section III, the theory of DTR and the model of DTR-OTS are presented. In section IV, the basic of fuzzy numbers and DTR calculation model considering fuzzy sets are presented. The performance results of DTR- and FDTR-OTS are presented in section V and VI, respectively, followed by discussions of the results in section VII. Finally, the paper is concluded in section VIII.

II. OPERATIONAL TRIPPING SCHEME

Conventionally, the OTS operates based on a set of pre- and post-fault states of power systems that have been pre-determined, together with a set of corrective actions to eliminate faults and return grids to stable conditions. The specific OTS considered in this paper is the generation rejection scheme (GRS), which trips generators after transmission line outages to prevent further unwanted cascading line outages, and this is possible as the tripping of specific generations would avoid sequential overloading on remaining lines, and instability altogether, and return grids to a secure operational state [23]. The GRS works by monitoring a set of transmission line circuit breakers, and it is only triggered to trip pre-defined generators when a certain combination of circuit breakers are opened (disconnected). As the operations of this GRS is fixed and respond based on the developments of events, it is also classified as the event-based OTS.

The advent of WAM system technology enables the deployments of synchronized measurement sensors, and this presents an unparalleled opportunity to improve monitoring and situational awareness of grid operations. With this, the event-based OTS that does not discriminate fault severity and may trigger excessively due to conservative and worst case assumptions of parameters, which is exactly the STR-OTS, can now operate more precisely in real-time and migrate to more targeted operations, such as the DTR-OTS, as proposed in this paper. Therefore, the benefits of capitalizing on the thermal security data of the protected transmission lines by DTR-OTS is demonstrated in this paper.

A. OTS of the Saudi Arabia national grid pilot zone

An existing GRS variant of the OTS that is used in the SA national grid is selected to exemplify and highlight the benefits of DTR-OTS. The pilot zone of the grid, at which the conventional STR-OTS is deployed is a group of seven 400kV substations, as shown in Fig. 1. Notice that the values of generation capacity and load demand shown in the figure are all maximum values. The connections outside of this pilot zone have been omitted from the figure as only power flows and statuses of line circuit breakers inside this zone are monitored by the OTS.

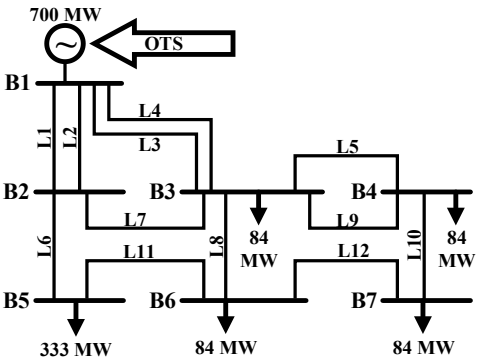

Fig. 1. Pilot zone of Saudi Arabia national grid where OTS is deployed and studied.

The STR-OTS monitors all lines in the pilot zone, and a pre-defined level of generations will be tripped if specific combinations of these monitored lines are disconnected. Therefore, the tripping action is pre-determined based on sequential developments of pre-selected contingencies. In other words, the operation of STR-OTS is fixed based on a set of chronological events. The purpose of the generation tripping is to reduce the distribution of load currents on the remaining un-faulted lines after the disconnections of faulted lines, so that the risk of cascade overloading on the remaining lines is reduced.

The presented OTS is designed to trip generation supply at bus B1 as only this bus hosts generators in the pilot zone. In the conventional STR-OTS, the statuses of line circuit breakers are the only inputs of the OTS, which will be analyzed and used to generate a trip-signal whenever three lines within the pilot zone are disconnected. This standard of operation is the N-2 criteria, whereby the grid is designed to continue to function normally even under two simultaneous contingencies. However, three or more simultaneous

This article has been accepted for publication in a future issue of this journal, but has not been fully edited. Content may change prior to final publication. Citation information: DOI 10.1109/ACCESS.2021.3086866, IEEE Access

contingencies may cause problems in the grid. In order to avoid erroneous tripping responses due to transient and sub-transient events, the trip signal will only take effects after an intentional delay of 0.1 s, which is reasonably longer than both of the transients.

A network of phasor measurement units (PMUs) and weather sensors are also available in the pilot zone, which can be used to obtain various power system and weather measurements, i.e., real-time line current flows, the statuses of line circuit breakers and environmental data, that are required for the implementation of DTR-OTS as part of the grid modernization efforts. The PMU is a state-of-the-art power system device that can digitally sample measurements of voltage and current phasors with very precise time tagging that are useful for synchronizations in a network of PMUs [38]. The role of this special zone is to create a test bed for studying and justifying the rollout of wide area PMUs in the SA grid to form an energy management system for various PMU enabled applications [39]. To simplify the studies presented here for the DTR-OTS, it is considered that sufficient PMUs are installed in the pilot zone to monitor the statuses and currents of all transmission lines.

B. Performance of the STR-OTS in SA national grid

Based on the existing STR-OTS system in Fig. 1, its performance is analysed and demonstrated here. During test, it is considered that all transmission lines are monitored, but only the following four critical lines, which carry the heaviest loading under normal condition (no contingency), are presented:

1. L1 & L2: 66.77 MW under normal condition
2. L6: 117.78 MW under normal condition
3. L8: 70.5 MW under normal condition

Case 1: Grid losses L3, L4 and L7 with the STR-OTS disabled.

In this case, the grid is rated based on the STR system and the lines L3, L4 and L7 are tripped at 400 s, 410 s, and 420 s, respectively, due to faults. The STR-OTS is disabled and there is no generation tripping to ease the additional loading burden that is transferred onto the remaining un-faulted lines when the three faulted lines are disconnected. The chronology of line loadings on L1 & L2, L6 and L8 is shown in Fig. 2.

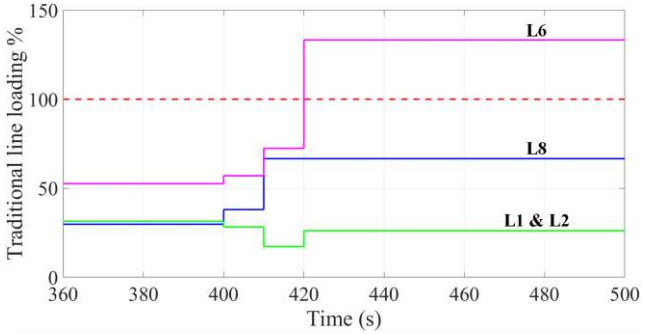

Fig. 2. Percentage current loadings on L1&L2, L6 and L8 for Case 1.

The results show that after the loss of three transmission lines, L6 exceeds 100% of its STR, and it is vulnerable to tripping due to high fault current, which risks overloading the remaining lines and eventually the grid is open to cascading outages. Therefore, corrective actions that are afforded by the OTS system is important to ensure that the grid is returned to normal stable conditions.

The case study above indicates that the pilot zone is vulnerable to cascading failures when three transmission lines are lost if there was no adequate protection system. Ensuring grid security due to severe contingencies, caused either by line failures, maintenance activities or a combination of both, is the role played by OTS and, in general, by other SIPS.

Case 2: Grid losses L3, L4 and L7 with the STR-OTS enabled.

Case 2 is similar to Case 1, except that the STR-OTS is now enabled. Upon the tripping of the third transmission line L7 at 420 s, the OTS is triggered after 0.1 s delay to trip power generation at bus B1 by 30%, and this corrective action returns the loading of all critical lines to values below 100% of their STRs, as shown in Fig. 3.

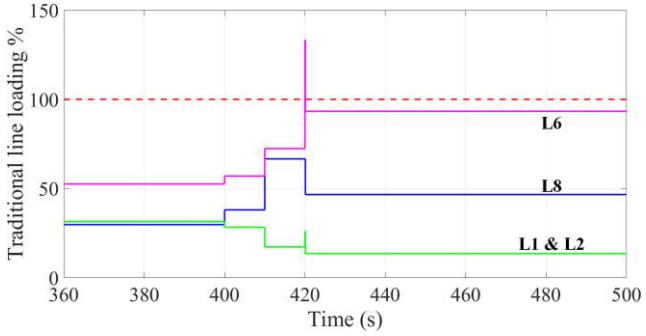

Fig. 3. Percentage current loadings on L1&L2, L6 and L8 for Case 2.

The illustration of the moment when the STR-OTS is triggered is enlarged and shown in Fig. 4, which shows that at 420 s, the STR-OTS is armed and ready to be triggered after L6 exceeds 100% of its STR due to the loss of three transmission lines, but is only triggered after 0.1 s delay to avoid erroneous respond, as mentioned earlier. The generation tripping at 420.1 s reduces loadings of all critical lines, and this successfully avoids the violation of static thermal limits, eliminates the risk of grid cascading outages and subsequently avoids system collapse. The line fault detection and STR-OTS triggering signals are also plotted, as shown in Fig. 5.

The STR-OTS is a simple operation, reliable, respond quickly, eliminates the risk of cascading outages and eventually grid collapse. Despite this, its deployment is still questionable. The reason is the lines rated with STRs are most likely still far from exceeding their maximum thermal

This article has been accepted for publication in a future issue of this journal, but has not been fully edited. Content may change prior to final publication. Citation information: DOI 10.1109/ACCESS.2021.3086866, IEEE Access

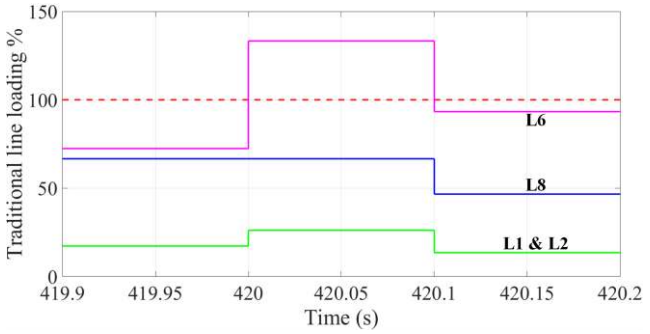

Fig. 4. Enlarged version of Fig. 3 between 419.9 s and 420.2 s.

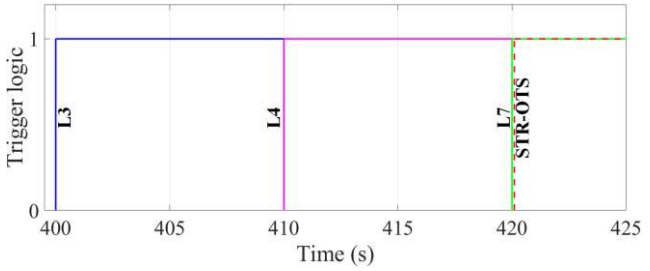

Fig. 5. Fault detection and triggering logics of Case 2.

capacity due to conservative weather assumptions in line rating calculations. Therefore, there is a high chance that STR-OTS causes an unnecessary number of tripping, which is costly and can create disturbances, such as complicating other systems that are otherwise stable.

At the time when the STR-OTS is triggered, actual line thermal capacities based on real-time weather conditions, as calculated by the DTR system, are most likely greater than the STR. Thus, under the DTR operation, the triggering of the OTS would have been avoided or delayed to a later time and, hence, lesser interruptions of power generations. With the advent of advanced and cost effective PMUs for WAM application, it is possible to implement the DTR- instead of the STR-OTS to avoid unnecessary tripping actions.

III. DTR-OTS

This paper proposes the integration of DTR system and OTS to form a novel DTR-OTS, which is possible due to WAM afforded by the deployment of PMUs. Existing PMUs and weather sensors along transmission lines in the pilot zone collect and stream data to a centralized monitoring and control unit, where DTRs are calculated and then line ratings are assigned. The uncertainty in the collection of these data are considered and, due to this, a study on the fuzzy version of the DTR-OTS, which is the FDTR-OTS, is also performed in this paper and is described in section IV.

A. Dynamic thermal rating system theory

The steady state DTR values of overhead lines, based on the IEEE 738 standard, is calculated as the following:

$$Q_c(T_c, T_a, V_w, \varphi) + Q_r(T_c, T_a) = Q_s(\omega) + I^2R(T_c), \quad (1)$$

where Q_c is the convection heat loss, Q_r is the radiation heat loss, Q_s is the radiation heat gain and $I^2R(T_c)$ is the joule heat gain due to current flow, I, where its maximum permissible value is the line rating. Each of this heat element is further calculated as a function of various weather data, which are wind speed, V_w, incident wind angle with respect to the line, φ, ambient temperature, T_a, solar angle, ω, and two conductor properties: conductor temperature, T_c, and conductor resistance, R, whose value is dependent on T_c.

The calculation of (1) depends on 14 inputs. Among them, the weather data vary frequently and may be subjected to sampling error due to inherent uncertainties of weather sensors. Although the remaining inputs, such as conductor properties, are fixed, the uncertainty of the weather data causes a chain of modifications in the execution of (1), which requires the implementation of fuzzy theory, and this is described in section IV.

Real-time variations of weather conditions, or changes in grid electrical properties, can cause instantaneous fluctuations of line rating values. However, the transition between values of conductor temperature is not instantaneous and instead undergo a delayed respond, as shown in Fig. 6.

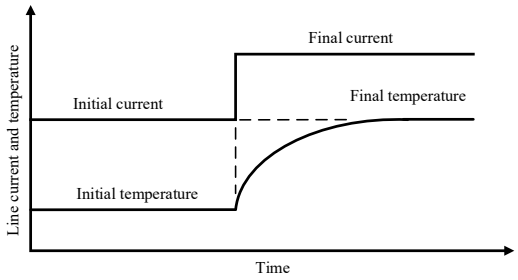

Fig. 6. Step changes of line current and temperature.

The figure shows that when the line loading value undergoes a step increase due to the disconnections of faulted lines, the ensuing increment of joule heating breaks the existing conductor steady state heat balance condition and, as a result, the conductor temperature rises steadily before reaches a new final equilibrium value. The rate at which the temperature changes depends on several factors such as initial and final line loadings and conductor temperatures and weather conditions. In short, Fig. 6 demonstrates a transient thermal response and, it is modelled as the following:

$$\frac{dT_c}{dt} = \frac{1}{mc_p}[R(T_c)I^2 + Q_s - Q_c - Q_r], \quad (2)$$

where mc_p is the total heat capacity of the conductor and t is time in second to show how long the transient response take place.

The time needed for the transient respond of conductor temperatures is the opportunity window capitalized by the DTR-OTS to delay the trigger of OTS and to avoid

This article has been accepted for publication in a future issue of this journal, but has not been fully edited. Content may change prior to final publication. Citation information: DOI 10.1109/ACCESS.2021.3086866, IEEE Access

unnecessary tripping action, which eventually improves the timing of the OTS trigger. Therefore, it is imperative that t is solved and this can be done using numerical integration methods, but finding a suitable elementary and antiderivative function is challenging. Instead of exact computation, a numerical approximation of the antiderivative is performed in this paper, and this is essentially the linearization of the non-steady-state heat balance equation given in (2).

According to [40], a method of approximating radiation cooling, Q_r, as a linear function of temperature was proposed. In doing so, and after considering a step change in electrical current, the transient thermal response is given as the following:

$$T_c(t) = T_i + \left(T_f - T_i\right)\left(1 - e^{-t/\tau}\right), \tag{3}$$

such that,

$$\tau = \frac{\left(T_f - T_i\right)mc_p}{R\left(T_{avg}\right) \times \left(I_f^2 - I_i^2\right)}, \tag{4}$$

where T_i is the initial steady-state conductor temperature before the step increase of electrical current, I_i and, T_f is the final steady-state conductor temperature after the step increase of electrical current, I_f. T_{avg} is the average conductor temperature, $\left(T_i + T_f\right)/2$, which the conductor resistance is based on.

Based on (3) and (4), conductor temperatures at each time step can be determined and the exact time needed to reach a particular temperature is known.

B. DTR-OTS architecture

The proposed DTR-OTS architecture is shown in Fig. 7, which shows that there is a real-time line loading block that collects actual current loading of transmission lines and, a real-time weather data block that collects real-time weather data. The variations of weather conditions along each transmission line are considered and hot spots of lines are duly identified, as it was found that weather data varies significantly along all the considered lines. Due to this, the minimum rating among all spans of a line determine the DTR of the entire line. The weather and line loading data of hot spots is used to solved (3) in the real-time temperature calculation block, which its output is the real-time conductor temperature, $T_c(t)$, and it is compared with the maximum permissible conductor temperature, $T_c(max)$, in the temperature comparison logic block. A tripping signal is generated after the 0.1 s delay whenever the limit of the permissible conductor temperature is exceeded, i.e., $T_c(t) > T_c(max)$.

Using the temperature comparison logic block, the DTR-OTS constantly determines whether the monitored transmission lines are overloaded and adaptively adjusts its tripping decisions. Prior to reaching the maximum conductor temperature, the DTR-OTS issues an alarm to provide warning to utilities that the existing current loading will heat the lines up to their maximum permissible conductor temperature and, eventually, exceeds the maximum temperature if no remedial action was taken. In this paper, the alarm signal is triggered whenever conductors are heated above 90% of their maximum designed temperature. This ensures utilities know that conductor temperatures are approaching levels that are dangerously close to their maximum values and, this is crucial as further undesirable changes in weather conditions can cause the lines to be very vulnerable to overloading. This alarm feature is only to enhance situational awareness on the operational risk of transmission lines, rather than to provide an automatic response, but it enables informed decision making to be taken to pre-empt problems and not responding only after faults have occurred.

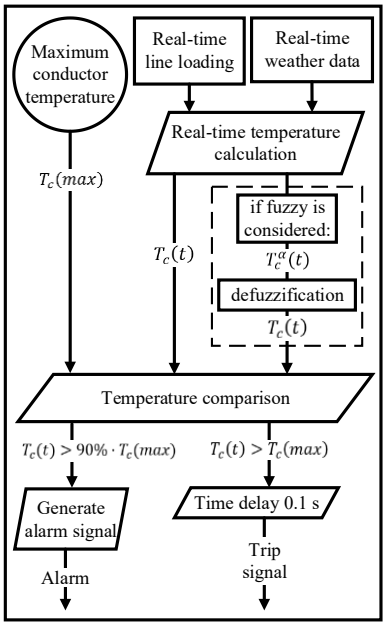

Fig. 7. DTR- and FDTR-OTS architectures.

The data mentioned above is collected through high accuracy PMUs and weather sensors available in the pilot zone. The main motivation of implementing the DTR-OTS is so that the triggering of protection system (generating tripping) is delayed and, the confidence for doing so stems from the synchronized nature of PMU measurements and precise time tagging that is available on each data sampled from across a wide area. These time tags reduce the uncertainty of the available time that the OTS can afford to delay before line thermal overloads occur and, no assumptions would have to be made on the relative time difference between each data. Moreover, the standardization of the PMU data under the IEEE C37.118.2 standard [41] is far simpler and organized than many existing non-uniform proprietary formats used for data exchange.

IV. FDTR-OTS

The proposed DTR-OTS in section III assumes that there is no error in sensors used for data sampling and, according

to fuzzy theory, the ensuing calculations are crisp values. On the contrary, when uncertainties are considered, analyses in the form of ranges of values are obtained, which are known as fuzzy numbers. In this section, the theory of fuzzy DTR is incorporated into the proposed DTR-OTS to form the fuzzy based version, known as the FDTR-OTS, as shown in Fig. 7. Despite the addition of the new fuzzy theory, all the models presented in section II and III are still applicable. The implementations of (1) to (4) still remain the same except that the steady state final and initial temperatures are now determined based on fuzzy numbers.

A. Basics of fuzzy numbers

One of the most important issues associated with fuzzy analyses is the computational efficiency, which can be achieved by composing membership functions into interval calculations [42]. The composition of each fuzzy interval is referred to as the α-cut and it is applied on fuzzy calculations to compute final results associated with the α-cut. Given a fuzzy number A, the α-cut of this fuzzy number is described as the following:

$$\begin{aligned}\forall\alpha \in [0,1]: A^{\alpha} &= \{x|\mu_A(x) \geq \alpha\} \\ &= [A_1^{\alpha}, A_2^{\alpha}] = [A_{\min}^{\alpha}, A_{\max}^{\alpha}],\end{aligned} \tag{5}$$

where $\mu_A(x)$ is the membership function of fuzzy number A.

In order to utilize the fuzzy results practically, they are converted into crisp numbers through a variety of "defuzzification" processes, such as magnitude [43], distance [44], centroid point (used in this paper) [45], and expected value [46]. The centroid point model is shown as the following:

$$\bar{x}(A) = \frac{\int_{a_1}^{a_2} x \cdot \mu_A(x)\, dx}{\int_{a_1}^{a_2} \mu_A(x)\, dx}, \tag{6}$$

where a_1 and a_2 are the limits of x for all non-zero membership grade of fuzzy number A.

B. Fuzzy DTR calculations

The transmission line heat balance equation in (1) has various input weather data, whose uncertainties are modelled by fuzzy numbers. Therefore, the calculations of fuzzy conductor temperatures are initiated by the fuzzification of these inputs. Weather data such as wind speed, V_w, wind angle, φ, ambient temperature, T_a and solar hour angle, ω, are all uncertain due to variations of time periods, and inaccuracies of their measurement devices. Hence, all these inputs are modelled by fuzzy numbers and their membership functions are $\mu_{T_a}(T_a)$, $\mu_{V_w}(V_w)$, $\mu_{\varphi}(\varphi)$ and $\mu_{\omega}(\omega)$, respectively. The fuzzification of these inputs changes (1) and equations embedded in), which are all described here:

1) fuzzy model of air density, ρ_f^{α}

The shape of fuzzy membership function is not affected by the sum and multiplication of crisp numbers. Therefore:

$$T_{film}^{\alpha} = \left[T_{film1}^{\alpha}, T_{film2}^{\alpha}\right] = \left[\frac{T_{a1}^{\alpha} + T_{c1}^{\alpha}}{2}, \frac{T_{a2}^{\alpha} + T_{c2}^{\alpha}}{2}\right], \tag{7}$$

where T_a is fuzzy. Then, the fuzzy air density, ρ_f^{α}, is as follow:

$$\begin{aligned}\rho_f^{\alpha} &= \left[\rho_{f1}^{\alpha}, \rho_{f2}^{\alpha}\right] \\ &= \left[\frac{H}{1 + 0.00367T_{film2}^{\alpha}}, \frac{H}{1 + 0.00367T_{film1}^{\alpha}}\right],\end{aligned} \tag{8}$$

such that,

$$H = 1.293 - 1.525 \times 10^{-4}H_e + 6.379 \times 10^{-9}H_e^2. \tag{9}$$

2) fuzzy model of air dynamic viscosity, μ_f^{α}

The mathematical operation of positive power only increases function values monotonically and can be directly applied onto the membership function of T_{film}^{α}. Therefore, the fuzzy air dynamic viscosity, μ_f^{α}, is as follow:

$$\begin{aligned}\mu_f^{\alpha} &= \left[\mu_{f1}^{\alpha}, \mu_{f2}^{\alpha}\right] \\ &= \begin{bmatrix}\dfrac{1.458 \times 10^{-6}\left(T_{film1}^{\alpha} + 273\right)^{1.5}}{T_{film2}^{\alpha} + 383.4}, \\ \dfrac{1.458 \times 10^{-6}\left(T_{film2}^{\alpha} + 273\right)^{1.5}}{T_{film1}^{\alpha} + 383.4}\end{bmatrix}.\end{aligned} \tag{10}$$

3) fuzzy model of air thermal conductivity, k_f^{α}

As mentioned earlier, the positive power is directly applied onto T_{film}^{α}. Therefore, the fuzzy air thermal conductivity, k_f^{α}, is as follow:

$$\begin{aligned}k_f^{\alpha} &= \left[k_{f1}^{\alpha}, k_{f2}^{\alpha}\right] \\ &= \begin{bmatrix}x_1 + x_2T_{film} - x_3\left(T_{film2}^{\alpha}\right)^2, \\ x_1 + x_2T_{film} - x_3\left(T_{film1}^{\alpha}\right)^2\end{bmatrix},\end{aligned} \tag{11}$$

where $x_1 = 0.02424$, $x_2 = 7.477 \times 10^{-5}$ and $x_3 = 4.407 \times 10^{-9}$.

4) fuzzy model of wind direction factor, k_{angle}^{α}

The fuzzy wind direction factor, k_{angle}^{α}, is as follow:

$$\begin{aligned}&k_{angle}^{\alpha} \\ &= \left[k_{angle1}^{\alpha}, k_{angle2}^{\alpha}\right] \\ &= \begin{bmatrix}y_1 + y_2\cos(2\varphi_1^{\alpha}) + y_3\sin(2\varphi_1^{\alpha}) - \cos(\varphi_2^{\alpha}), \\ y_1 + y_2\cos(2\varphi_2^{\alpha}) + y_3\sin(2\varphi_2^{\alpha}) - \cos(\varphi_1^{\alpha})\end{bmatrix},\end{aligned} \tag{12}$$

where $y_1 = 1.194$, $y_2 = 0.194$ and $y_3 = 0.368$.

Notice that $0° \leq \varphi \leq 90°$, and when the crisp value of k_{angle} is calculated by ignoring fuzzy operation, that is applying only either 0° (minimum) or 90° (maximum) in (12), the range $0.388 \leq k_{angle} \leq 1$ is obtained. However, when the fuzzy trigonometry as shown in (12) is reinstated, the range $0 \leq k_{angle} \leq 1.39$ is obtained instead and this lies outside of the crisp acceptable range. To overcome this, the range of k_{angle}^{α} is always truncated to the crisp acceptable range only. For example, when $30° \leq \varphi \leq 60°$ with

This article has been accepted for publication in a future issue of this journal, but has not been fully edited. Content may change prior to final publication. Citation information: DOI 10.1109/ACCESS.2021.3086866, IEEE Access

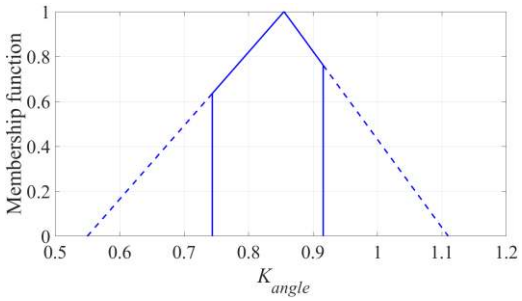

Fig. 8. Range of fuzzy numbers is truncated to within the crisp acceptable range

triangular membership function, the crisp k_{angle} values are calculated to be in between 0.74 and 0.92, which are the possible minimum and maximum values of k_{angle}. However, when fuzzy mathematics as shown in (12) are applied, the range of k_{angle} is in between 0.55 and 1.11 instead. As the range based on fuzzy numbers is larger than the range based on crisp numbers, the resultant fuzzy k_{angle}^{α} is truncated to within the crisp acceptable range only, as shown by the bold lines in Fig. 8.

5) fuzzy model of convection heat loss rate, Q_c^{α}

The fuzzy convection heat loss rate, Q_c^{α}, is as follow:

$$\begin{aligned} Q_c^{\alpha} &= [Q_{c1}^{\alpha}, Q_{c2}^{\alpha}] \\ &= \begin{bmatrix} \max(q_{cH1}^{\alpha}, q_{cL1}^{\alpha}, q_{cN1}^{\alpha}), \\ \max(q_{cH2}^{\alpha}, q_{cL2}^{\alpha}, q_{cN2}^{\alpha}) \end{bmatrix}, \end{aligned} \tag{13}$$

such that,

$$\begin{aligned} q_{cH}^{\alpha} &= [q_{cH1}^{\alpha}, q_{cH2}^{\alpha}] \\ &= \begin{bmatrix} (1.01 + 0.0372(\lambda_1^{\alpha})^{0.52}) \cdot \gamma_1^{\alpha}, \\ (1.01 + 0.0372(\lambda_2^{\alpha})^{0.52}) \cdot \gamma_2^{\alpha} \end{bmatrix}, \end{aligned} \tag{14}$$

$$\begin{aligned} q_{cL}^{\alpha} &= [q_{cL1}^{\alpha}, q_{cL2}^{\alpha}] \\ &= \begin{bmatrix} (0.0119(\lambda_1^{\alpha})^{0.6}) \cdot \gamma_1^{\alpha}, \\ (0.0119(\lambda_2^{\alpha})^{0.6}) \cdot \gamma_2^{\alpha} \end{bmatrix}, \end{aligned} \tag{15}$$

$$\begin{aligned} q_{cN}^{\alpha} &= [q_{cN1}^{\alpha}, q_{cN2}^{\alpha}] \\ &= \begin{bmatrix} 0.0205D^{0.75}(\rho_{f1}^{\alpha})^{0.5}(T_{c1}^{\alpha} - T_{a2}^{\alpha})^{1.25}, \\ 0.0205D^{0.75}(\rho_{f2}^{\alpha})^{0.5}(T_{c2}^{\alpha} - T_{a1}^{\alpha})^{1.25} \end{bmatrix}, \end{aligned} \tag{16}$$

where,

$$\begin{aligned} \lambda^{\alpha} &= [\lambda_1^{\alpha}, \lambda_2^{\alpha}] \\ &= \left[D\frac{\rho_{f1}^{\alpha} V_{w1}^{\alpha}}{\mu_{f2}^{\alpha}}, D\frac{\rho_{f2}^{\alpha} V_{w2}^{\alpha}}{\mu_{f1}^{\alpha}} \right], \end{aligned} \tag{17}$$

$$\begin{aligned} \gamma^{\alpha} &= [\gamma_1^{\alpha}, \gamma_2^{\alpha}] \\ &= \begin{bmatrix} (k_{angle1}^{\alpha} \cdot k_{f1}^{\alpha}) \cdot (T_{c1}^{\alpha} - T_{a2}^{\alpha}), \\ (k_{angle2}^{\alpha} \cdot k_{f2}^{\alpha}) \cdot (T_{c2}^{\alpha} - T_{a1}^{\alpha}) \end{bmatrix}, \end{aligned} \tag{18}$$

6) fuzzy model of radiation heat loss rate, Q_r^{α}

The fuzzy radiation heat loss rate, Q_r^{α}, is as follow:

$$\begin{aligned} Q_r^{\alpha} &= [Q_{r1}^{\alpha}, Q_{r2}^{\alpha}] \\ &= \begin{bmatrix} 0.0178D\varepsilon\left(\left(\frac{T_{c1}^{\alpha}+273}{100}\right)^4 - \left(\frac{T_{a2}^{\alpha}+273}{100}\right)^4\right), \\ 0.0178D\varepsilon\left(\left(\frac{T_{c2}^{\alpha}+273}{100}\right)^4 - \left(\frac{T_{a1}^{\alpha}+273}{100}\right)^4\right) \end{bmatrix}, \end{aligned} \tag{19}$$

7) fuzzy model of solar heat gain rate, Q_s^{α}

The same fuzzy trigonometry concept described for the calculation of k_{angle}^{α} is applicable here. The calculation of fuzzy solar heat gain rate, Q_s^{α}, begins as follow:

$$\begin{aligned} H_c^{\alpha} &= [H_{c1}^{\alpha}, H_{c2}^{\alpha}] \\ &= \begin{bmatrix} \arcsin\left(\begin{matrix}\cos(Lat)\cos(\delta)\cos(\omega_1^{\alpha}) \\ +\sin(Lat)\sin(\delta)\end{matrix}\right), \\ \arcsin\left(\begin{matrix}\cos(Lat)\cos(\delta)\cos(\omega_2^{\alpha}) \\ +\sin(Lat)\sin(\delta)\end{matrix}\right) \end{bmatrix}, \end{aligned} \tag{20}$$

$$\begin{aligned} Q_{se}^{\alpha} &= [Q_{se1}^{\alpha}, Q_{se2}^{\alpha}] \\ &= [k_{solar} q_{s1}^{\alpha}, k_{solar} q_{s2}^{\alpha}] \end{aligned} \tag{21}$$

such that,

$$\begin{aligned} q_s^{\alpha} &= [q_{s1}^{\alpha}, q_{s2}^{\alpha}] \\ &= \begin{bmatrix} \left(\begin{matrix} m_1 + m_2 H_{c1}^{\alpha} + m_3 (H_{c1}^{\alpha})^2 \\ + m_4 (H_{c1}^{\alpha})^3 + m_5 (H_{c1}^{\alpha})^4 \\ + m_6 (H_{c1}^{\alpha})^5 + m_7 (H_{c1}^{\alpha})^6 \end{matrix}\right), \\ \left(\begin{matrix} m_1 + m_2 H_{c2}^{\alpha} + m_3 (H_{c2}^{\alpha})^2 \\ + m_4 (H_{c2}^{\alpha})^3 + m_5 (H_{c2}^{\alpha})^4 \\ + m_6 (H_{c2}^{\alpha})^5 + m_7 (H_{c2}^{\alpha})^6 \end{matrix}\right) \end{bmatrix} \end{aligned} \tag{22}$$

where $m_1, m_2, \ldots, m_7$ are constants available in the IEEE 738 standard.

Consider also the followings:

$$\begin{aligned} Z_c^{\alpha} &= [Z_{c1}^{\alpha}, Z_{c2}^{\alpha}] \\ &= [C + \arctan(\chi_1^{\alpha}), C + \arctan(\chi_2^{\alpha})], \end{aligned} \tag{23}$$

such that,

$$\begin{aligned} \chi^{\alpha} &= [\chi_1^{\alpha}, \chi_2^{\alpha}] \\ &= \begin{bmatrix} \dfrac{\sin(\omega_1^{\alpha})}{\sin(Lat)\cos(\omega_2^{\alpha}) - \cos(Lat)\tan(\delta)}, \\ \dfrac{\sin(\omega_2^{\alpha})}{\sin(Lat)\cos(\omega_1^{\alpha}) - \cos(Lat)\tan(\delta)} \end{bmatrix}, \end{aligned} \tag{24}$$

where the solar azimuth constant C is a function of the fuzzy solar hour angle, ω^{α}, and solar azimuth χ which can be estimated from the table shown in IEEE 738 standard.

Next, consider also the following:

$$\begin{aligned} \theta^{\alpha} &= [\theta_1^{\alpha}, \theta_2^{\alpha}] \\ &= \begin{bmatrix} \arccos(\cos(H_{c1}^{\alpha})\cos(Z_{c1}^{\alpha} - Z_l)), \\ \arccos(\cos(H_{c2}^{\alpha})\cos(Z_{c2}^{\alpha} - Z_l)) \end{bmatrix}, \end{aligned} \tag{25}$$

and finally,

This article has been accepted for publication in a future issue of this journal, but has not been fully edited. Content may change prior to final publication. Citation information: DOI 10.1109/ACCESS.2021.3086866, IEEE Access

$$Q_s^\alpha = [Q_{s1}^\alpha, Q_{s2}^\alpha] = [\psi Ar Q_{se1}^\alpha \sin(\theta_1^\alpha), \psi Ar Q_{se2}^\alpha \sin(\theta_2^\alpha)], \quad (26)$$

Due to trigonometry operations, values of Q_s^α that fall outside of its acceptable crisp range are removed, which is an approach that is similar to handling the final range of k_{angle}^α.

8) fuzzy model of conductor temperature, T_c^α

Considering all the earlier fuzzy parameters, the fuzzy conductor temperature is calculated by rearranging (1) as follow:

$$T_c^\alpha = [T_{c1}^\alpha, T_{c2}^\alpha] = \begin{bmatrix} \left(\frac{Q_{c1}^\alpha + Q_{r1}^\alpha - Q_{s2}^\alpha}{I^2} - R(T_L)\right) r + T_L, \\ \left(\frac{Q_{c2}^\alpha + Q_{r2}^\alpha - Q_{s1}^\alpha}{I^2} - R(T_L)\right) r + T_L \end{bmatrix}, \quad (27)$$

such that,

$$\begin{Bmatrix} T_i^\alpha = [T_{i1}^\alpha, T_{i2}^\alpha], \\ T_f^\alpha = [T_{f1}^\alpha, T_{f2}^\alpha] \end{Bmatrix} \in \{T_c^\alpha\} \quad (28)$$

$$r = \left(\frac{T_H - T_L}{R(T_H) - R(T_L)}\right) \quad (29)$$

where the line current, I, corresponds to either the initial current, I_i, or final current, I_f, before and after step increase of currents, respectively. In the former correspondence, T_i^α is obtained and in the latter, T_f^α is obtained instead.

Finally, the minimum conductor temperature among all spans of a line is selected as the final temperature of the conductor, such as follow:

$$T_c^\alpha = \min(T_{c,s1}^\alpha, T_{c,s2}^\alpha, \dots, T_{c,sN}^\alpha) \quad (30)$$

The formulations presented above are comprehensive and applicable on all forms of membership functions, i.e., triangular, rectangular, Gaussian and etc. The selection of the appropriate membership function though, depends on expert knowledge, historical record data, the accuracy of measuring devices and data sampling period and operating conditions. For the purpose of simplicity, this paper utilizes only triangular membership function on all fuzzy parameters mentioned previously.

The response time of conductor temperature in (3) and (4) after considering the above fuzzy parameters are modified and becomes:

$$T_c(t)^\alpha = [T_c(t)_1^\alpha, T_c(t)_2^\alpha] = \begin{bmatrix} T_{i1}^\alpha + \left(T_{f1}^\alpha - T_{i1}^\alpha\right)\left(1 - e^{-(t/\tau_1^\alpha)}\right), \\ T_{i2}^\alpha + \left(T_{f2}^\alpha - T_{i2}^\alpha\right)\left(1 - e^{-(t/\tau_2^\alpha)}\right) \end{bmatrix} \quad (31)$$

such that,

$$\tau^\alpha = [\tau_1^\alpha, \tau_2^\alpha] = \begin{bmatrix} \frac{\left(T_{f1}^\alpha - T_{i1}^\alpha\right) mc_p}{R\left(T_{i1}^\alpha + T_{f1}^\alpha/2\right) \times \left(I_f^2 - I_i^2\right)}, \\ \frac{\left(T_{f2}^\alpha - T_{i2}^\alpha\right) mc_p}{R\left(T_{i2}^\alpha + T_{f2}^\alpha/2\right) \times \left(I_f^2 - I_i^2\right)} \end{bmatrix}, \quad (32)$$

V. PERFORMANCE OF THE DTR-OTS

Two case studies, namely case 3 and case 4, are presented here to demonstrate the superiority of DTR-OTS over the STR-OTS on the same network (Fig. 1). Note that in the DTR-OTS, the uncertainties of data are not considered and all sensors are assumed to be completely accurate.

Case 3: Grid losses L3, L4 and L7 with the DTR-OTS enabled.

In this case, the pilot zone losses line L3, L4 and L7 at 400 s, 410 s and 420 s, respectively, similar to scenarios of case 1 and 2, except that this time the DTR-OTS is armed instead of the STR-OTS. The average weather data over 20 years, from 1996 to 2016, which are used for DTR calculations, are obtained from the Saudi Arabia open data portal [47]. The resolution of the data is 360 s as weather conditions are generally stable within this period. The data is also from the summer days so that the studies performed here are based on the hottest season throughout a year.

The line fault detection and OTS triggering logics of Case 3 is shown in Fig. 9, which shows that despite losing three transmission lines, the DTR-OTS is not triggered because its temperature comparison logic block (Fig. 7) does not approve the trigger.

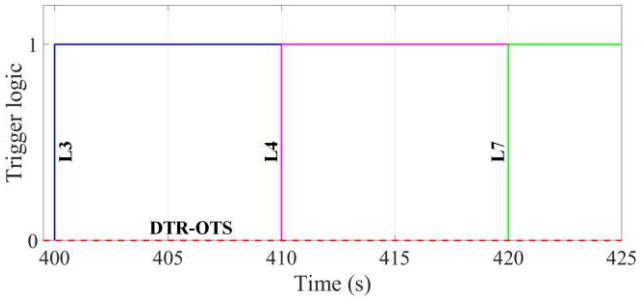

Fig. 9. Fault detection and triggering logics of Case 3.

This is in contrast with case 2 where the STR-OTS was triggered to trip 30% of generation capacity at B1. Due to this, the line loading percentages of the remaining lines (L1&L2, L6 and L8) continue to increase and finally L6 is loaded beyond 100% of its traditional line rating, as shown in Fig. 10.

This is acceptable because the maximum 70°C conductor temperature limit (the standard used in the pilot zone) of the

This article has been accepted for publication in a future issue of this journal, but has not been fully edited. Content may change prior to final publication. Citation information: DOI 10.1109/ACCESS.2021.3086866, IEEE Access

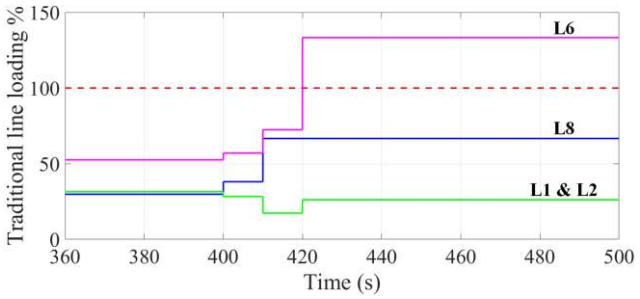

Fig. 10. Percentage current loadings on L1&L2, L6 and L8 for Case 3.

remaining lines is not yet violated even after the DTR-OTS detected the loss of three transmission lines. The temperature profiles of L1&L2, L6 and L8 as illustrated in Fig. 11 and, the comparisons between their DTRs and loadings as shown in Fig. 12(a)-(c), demonstrate that the decision not to trip generations at B1 is correct and justifiable. The fluctuations of values in these two figures are due to weather conditions that vary every 360 s and the DTR limits are calculated based on the maximum allowable conductor temperature of 70℃.

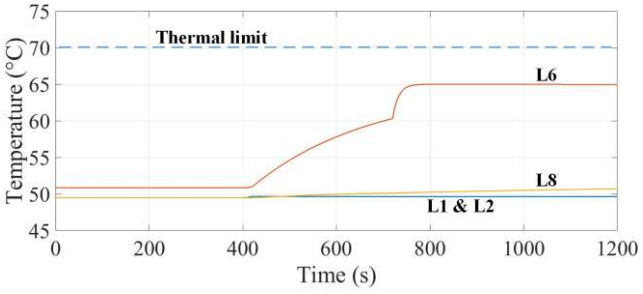

Fig. 11. Conductor temperatures of L1&L2, L6 and L8 for Case 3.

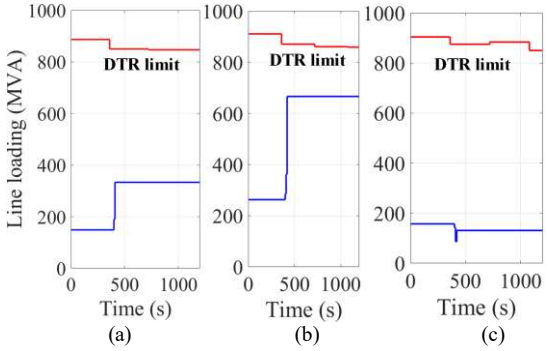

Fig. 12. DTRs and loadings of (a) L1&L2, (b) L6 and (c) L8 for Case 3.

Fig. 11 shows the delay response of conductor temperatures after several step increases of current loadings due to the loss of transmission lines. It shows that there is no violation of conductor temperature limit of 70℃ and that all conductors are still operating safely well within their designed thermal limits. This means that it is safe to continue loading the lines at the current levels after the detection of faults without having to trip generations. The 70℃ thermal limit is predetermined based on the profile provided by the conductor manufacturer. Fig. 12 reinforces the phenomenon of Fig. 11, whereby it shows that current loadings of all lines never exceed their DTR limits and therefore their conductor temperatures will never reach 70℃. Results of these two figures show that the proposed DTR-OTS is reliable and can prevent unnecessary tripping.

It is noted that changing the conductor temperature limit will affect decisions of the DTR-OTS and that the appropriate response by the OTS depends on the selection of a suitable level of this temperature limit. Thermal limits that are too high may prevent the OTS from ever tripping generations when necessary and expose lines to overloading, subsequently risking grid security. On the other hand, limits that are too low may cause unnecessary generation tripping which would lead to power supply inadequacy.

Case 4: Grid losses L5, L8 and L9 with the DTR-OTS enabled.

In this case, the pilot zone losses L5, L8 and L9 at 400 s, 410 s and 420 s, respectively, while the DTR-OTS is armed. The responses of current loadings on L1&L2, L6 and L8 along with their respective DTR limits are shown in Fig. 13(a)-(c), which shows that immediately after losing the third line, L6 is loaded up to above its DTR limits.

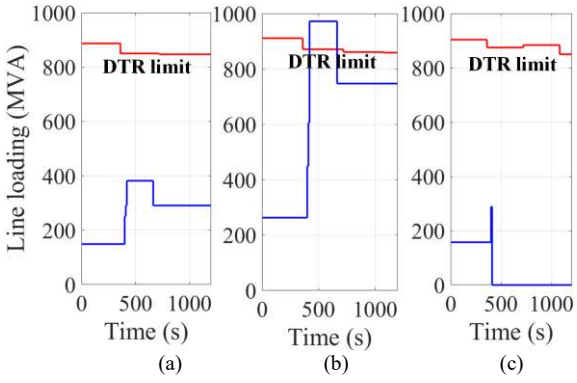

Fig. 13. DTRs and loadings of (a) L1&L2, (b) L6 and (c) L8 for Case 4.

However, due to the delay response of conductor temperatures, the current overloading sustain by L6 is maintained for another 244 s before the DTR-OTS triggers a generation tripping at 664 s in order to reduce the current loading on L6 to below its DTR limit, as shown in Fig. 13(b). Notice that as L8 is disconnected at 420 s, its current loading is completely reduced to zero at this time, as shown in Fig. 13(c). The line loadings on all these conductors are also expressed as a percentage of the traditional line loading as shown in Fig. 14 and, the fault detection and OTS triggering logics are shown in Fig. 15.

Next, the temperature profiles of all these lines are shown in Fig. 16. The figure shows that at 420 s, which is when after the pilot zone losses three lines, the conductor temperature of L6 rises exponentially until it reaches 70℃ at 664 s. At this time, the armed DTR-OTS is triggered to trip generation at B1 by 30%. Due to this, all line current loadings are

This article has been accepted for publication in a future issue of this journal, but has not been fully edited. Content may change prior to final publication. Citation information: DOI 10.1109/ACCESS.2021.3086866, IEEE Access

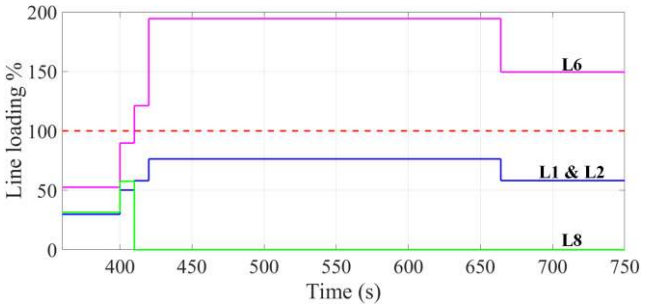

Fig. 14. Percentage of current loadings on L1&L2, L6 and L8 for Case 4

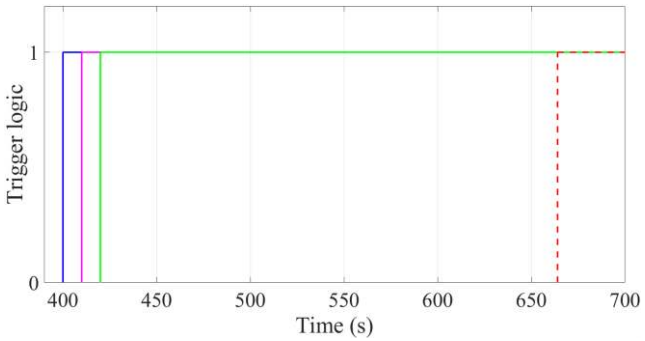

Fig. 15. Fault detection and DTR-OTS trigger logics of Case 4.

reduced and the temperature of L6 drops. The fluctuations of temperature values throughout the examination period are due to variations of weather conditions at every 360 s.

Notice at 545 s, when the conductor temperature of L6 reaches 63℃, an alarm signal is generated to warn utilities that the conductor temperature is already 10% away from reaching 70℃, which is the maximum permissible conductor temperature, and this is dangerously close to exceeding line thermal limit. As a result, situational awareness is enhanced and more informed decision is afforded. This alarm feature is possible due to the temperature comparison logic block available in the proposed DTR-OTS architecture.

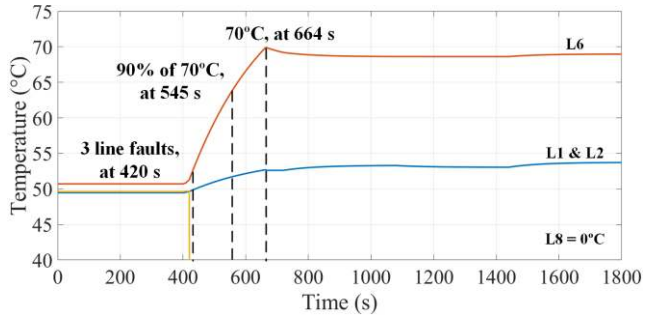

Fig. 16. Conductor temperatures of L1&L2, L6 and L8 for Case 4.

VI. PERFORMANCE OF THE FDTR-OTS

In this section, the uncertainties of weather data are considered and fuzzy DTR calculations (section IV.B) are performed. In order to demonstrate fuzzy effects toward the OTS, case 4 is extended to incorporate data uncertainties, which is now known as case 5, to demonstrate the operations of FDTR-OTS.

A triangular membership function is considered for all fuzzy weather data. The middle values of all the data membership functions are considered to be crisp values, which they have been used in the operation of the DTR-OTS where fuzzy numbers are not considered, as shown in the previous section.

The considered membership function has a base width of $\pm 20\%$, which means that when the uncertainty is the greatest at the α-cut of 0, the sampled data has the $\pm 20\%$ range. As the level of the α-cut moves up to 1, which is when no uncertainty is considered, the upper- and lower-range values converge and meet in the middle. A lower level of confidence towards a particular data uncertainty is reflected by a lower level of the α-cut to form a wider data range and vice versa. Hence, the α-cut of 1 (crisp value) represents that there is no error in the measurement sensors and, the α-cut of 0 represents the biggest possible error that the measuring sensors can have.

Case 5 (fuzzy): Grid losses L5, L8 and L9 with the FDTR-OTS enabled.

In this case, the pilot zone losses L5, L8 and L9 at 400 s, 410 s and 420 s, respectively, while the FDTR-OTS is armed. The α-cut of 0.5 is considered for all data, which means that the uncertainty of all data has the $\pm 10\%$ range. As it was shown earlier in case 4 that only L6 demonstrates line overloading after the loss three transmission lines, the effects of data uncertainty toward line loadings and DTR limits of L6 are presented only, as shown in Fig. 17(a) and (b) below.

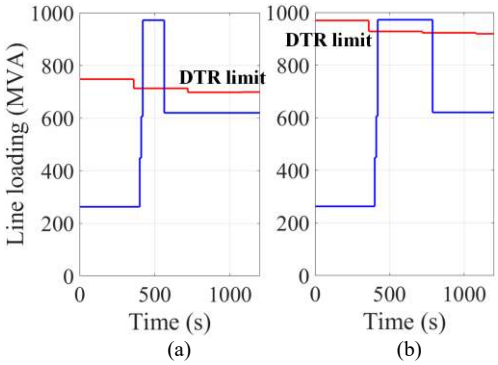

Fig. 17. DTRs and loadings of L6 in (a) worst (-10%) and (b) best (+10%) weather data range.

Fig. 17(a) and (b) are the cases when the worst (low wind speed, low wind angle, high ambient temperature, high solar radiation) and best (high wind speed, high wind angle, low ambient temperature, low solar radiation) weather data ranges are used, respectively. Due to this, the DTR limit of Fig. 17(a) is lower than that of Fig. 17(b). Both figures show that L6 is overloaded after losing three lines irrespective of which set of weather conditions is used. However, the overloading shown in Fig. 17(a) is sustained shorter than that

This article has been accepted for publication in a future issue of this journal, but has not been fully edited. Content may change prior to final publication. Citation information: DOI 10.1109/ACCESS.2021.3086866, IEEE Access

of Fig. 17(b), and this is due to the delay response of conductor temperatures, as shown in Fig. 18.

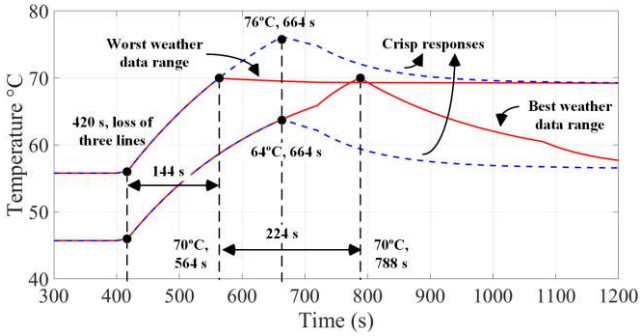

Fig. 18. Conductor temperature responses of L6 based on worst and best weather data range.

The figure shows that the FDTR-OTS with the worst weather data range is triggered at 564 s, which is 144 s after losing three transmission lines. While in the case with the best weather data range, the FDTR-OTS is triggered at 788 s, which is an additional delay of 224 s later than the worst case.

The analysis of Fig. 18 provides utilities with a range of options (between 564 s and 788 s) to decide the best timing to trigger the OTS. The most conservative option is to trigger the FDTR-OTS at 564 s to avoid any line overloading at all. However, selecting this option might cause the loss of up to 224 s of additional full power generations should the actual weather conditions be better than the weather data range considered in this option. On the other hand, selecting 788 s would ensure maximum power generation for the longest time, but this option risks overloading the lines if actual weather conditions turn out to be worse than the weather data range considered in this option.

In order to provide a useful solution, the fuzzy trigger time of FDTR-OTS is defuzzified based on the centroid point defuzzification method given in (6) to obtain a crisp trigger time. As a triangular membership function is used to model the uncertainties of all weather data, the output membership functions of the fuzzy trigger time can only be in the triangular form. Due to the symmetry of the triangular membership function, applying the proposed centroid point defuzzification on the triangular membership function to obtain the crisp trigger time produces the middle value of the function itself. As it is mentioned earlier that the middle values of all membership functions of this study are considered to be crisp values as well, the crisp trigger time (middle value) obtained through the defuzzification method is therefore the same as the trigger time of the DTR-OTS shown in Fig. 16 (664 s), where uncertainties are not considered and only the middle values are used.

Implementing this crisp trigger time on the FDTR-OTS based on the two extreme ranges of weather data produces two new delay responses of conductor temperature as shown by the two dash lines in Fig. 18. It shows that when the crisp trigger time is applied on the worst weather data range, line L6 is overloaded and its conductor temperature rises to 76℃ before tapering off. On the other hand, when the crisp trigger time is applied on the best weather data range, line L6 is loaded up to 64℃ only before the OTS is triggered to trip 30% of power generation at bus B1. The crisp trigger time represents the compromise that are neither too early (564 s) nor too late (788 s), which utilities can select to optimize the trigger time of their OTS. Such an option is only afforded in the FDTR-OTS where fuzzy numbers are analysed. The percentage of current loadings on L6 is shown in Fig. 19 and the fault detection and triggering logics of FDTR-OTS are shown in Fig. 20.

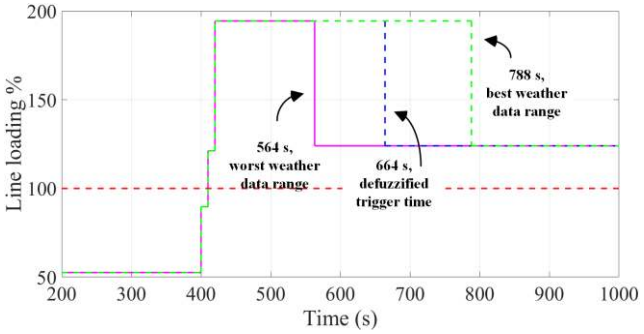

Fig. 19. Percentage of current loadings on L6 for Case 5.

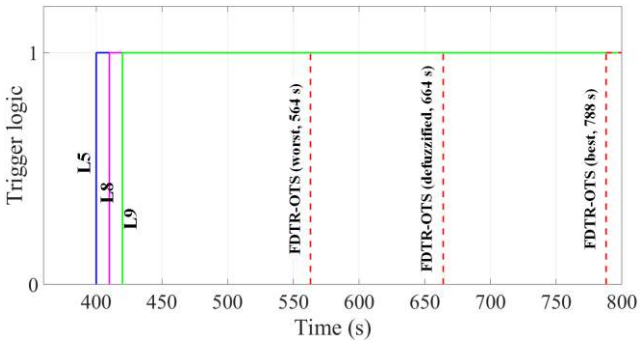

Fig. 20. Fault detection and DTR-OTS trigger logics of Case 5.

The reason the crisp trigger time of FDTR-OTS obtained by the defuzzification method is similar to the trigger time of DTR-OTS is only because all uncertainties of weather data are modelled using the triangular membership function. In practice, different types of membership functions for each group of weather data can be specifically selected based on expert meteorological and geographical knowledge. Such an approach will most likely produce various types of input membership functions based on locations, seasonality, data size, sampling methods and etc., which are all not considered in this study. The diversity of input membership functions will produce non-standard output membership functions that are most likely not symmetrical, and then the crisp trigger time obtained by the defuzzification method will be different from the trigger time without data uncertainties.

This article has been accepted for publication in a future issue of this journal, but has not been fully edited. Content may change prior to final publication. Citation information: DOI 10.1109/ACCESS.2021.3086866, IEEE Access

VII. DISCUSSIONS

The delay tripping of generations in both the DTR- and FDTR-OTS does not increase the risk of system security, as they use DTR technology to estimate the actual time of thermal overload. The temperature comparison logic block in both of the OTSs identifies whether thermal overload will occur in the future and when the overload will take place. As such, no immediate tripping is necessary whenever there is a loss of three transmission lines as there is no risk of line overloading yet. Hence, this situational awareness enables the strategic planning of a tripping time in advance of any line overload that might lead to cascade failures. Whenever possible, the time estimated for line overloading to occur can be used to schedule appropriate generation re-dispatches to alleviate overloading entirely, and subsequently avoid the need for generation tripping.

This available time is only useful if utilities can be informed of any imminent threats and be provided with the required information to make strategic decision in a timely fashion, which is precisely the role of the proposed DTR- and FDTR-OTS. They generate alarm signal to indicate imminent threats, provide estimations of time to thermal violation so that utilities have opportunities to relieve transmission line overload without resorting to generation tripping and, as the final option, authorise automated generation tripping when needed. The delay responses of conductor temperature, due to the exploitation of the conductor large thermal constant, as in both DTR- and FDTR-OTS, demonstrate that high speed protection systems that are commonly deployed in power system are not necessary.

The uncertainties considered in the FDTR-OTS offer additional values in that utilities are given a range of time to response to potential thermal overload, instead of only a single time which is estimated based on the assumption that sensors are perfect, which in reality is not. The disadvantage of assuming perfect sensors is that measurement errors that have been factored into the sampled data are not accounted for, and inappropriate trigger times may be assigned; if the trigger time is slower than the actual one, then line overloading will occur; on the other hand, if the trigger time is faster than it should be, then the line is not fully utilised and there is a greater inadequacy of power supply. Although the fuzzy properties considered in the FDTR-OTS enable the modelling of practical sensor behaviours, more statistical analyses of the sampled weather data are still needed to identify even more appropriate membership functions, so that the output membership functions can accurately represent actual conditions.

VIII. CONCLUSIONS

The OTS and specifically the proposed DTR- and FDTR-OTS are designed to preserve power system integrity as a whole rather than clearing individual faults. The OTSs that are presented in this paper help to eliminate network congestions by tripping power generations when required, and have the spillover effect of enabling more renewable integrations to achieve a low carbon network.

This paper demonstrates the benefit of integrating DTR into the existing STR-OTS and migrate to a more strategic operational tripping scheme. The proposed system takes advantage of the larger thermal over electrical time constants to delay the issuing of trip signals, generate alarm signals before the violation of conductor maximum temperature to improve situational awareness, and reduces the number of unnecessary tripping, all without compromising system security. The newly gain situational awareness also affords utilities to identify more efficient and less drastic solutions than the generation tripping. Moreover, grids equipped with the DTR system are also more flexible as the system allows line ratings to be flexibly adapted to the prevailing weather conditions, instead of fixed based on worst case assumptions.

The inherent uncertainties of weather sensors are accounted for in the FDTR-OTS. Analyses of this system show that the tripping of generations is not fixed on a particular time, rather, it can be performed between a range of time. The identification of appropriate input membership functions is important to ensure accurate output membership functions and crisp trigger time obtained by the defuzzification method. No methodology is devised to identify the membership function as this is outside the scope of this paper. The defuzzified crisp trigger time can approach the true yet, elusive trigger time if the technologies of sensors are enhanced to be more accurate.

The proposed OTS requires real-time data to operate and therefore adequate support of communication channel is critical, which its reliability can be considered in future work.

REFERENCES

[1] W. C. Khoo, J. Teh, and C. -M. Lai, "Integration of Wind and Demand Response for Optimum Generation Reliability, Cost and Carbon Emission," *IEEE Access*, vol. 8, pp. 183606–183618, 2020, doi: 10.1109/ACCESS.2020.3029273.

[2] M. K. Metwaly and J. Teh, "Optimum Network Ageing and Battery Sizing for Improved Wind Penetration and Reliability," *IEEE Access*, vol. 8, pp. 118603–118611, 2020, doi: 10.1109/ACCESS.2020.3005676.

[3] F. Mohamad, J. Teh, and H. Abunima, "Multi-Objective Optimization of Solar/Wind Penetration in Power Generation Systems," *IEEE Access*, vol. 7, pp. 169094–169106, 2019, doi: 10.1109/access.2019.2955112.

[4] J. Teh, C.-M. Lai, and Y.-H. Cheng, "Improving the Penetration of Wind Power with Dynamic Thermal Rating System, Static VAR Compensator and Multi-Objective Genetic Algorithm," *Energies*, vol. 11, no. 4, 2018, doi: 10.3390/en11040815.

[5] H. Abunima and J. Teh, "Reliability Modeling of PV Systems Based on Time-Varying Failure Rates," *IEEE Access*, vol. 8, pp. 14367–14376, 2020, doi: 10.1109/access.2020.2966922.

[6] H. Abunima, J. Teh, and H. J. Jabir, "A New Solar Radiation Model for a Power System Reliability Study," *IEEE Access*, vol. 7, pp. 64758–64766, 2019, doi: 10.1109/access.2019.2916168.

[7] L. Alhafadhi and J. Teh, "Advances in reduction of total harmonic distortion in solar photovoltaic systems: A literature review," *Int. J. Energy Res.*, vol. n/a, no. n/a, Dec. 2019, doi: 10.1002/er.5075.

[8] L. Alhafadhi, J. Teh, C.-M. Lai, and M. Salem, "Predictive Adaptive Filter for Reducing Total Harmonics Distortion in PV Systems," *Energies*, vol. 13, no. 12, 2020, doi: 10.3390/en13123286.

[9] F. Mohamad, J. Teh, C.-M. Lai, and L.-R. Chen, "Development of Energy Storage Systems for Power Network Reliability: A Review," *Energies*, vol. 11, no. 9, 2018, doi: 10.3390/en11092278.

[10] F. Mohamad and J. Teh, "Impacts of Energy Storage System on Power System Reliability: A Systematic Review," *Energies*, vol. 11, no. 7, 2018, doi: 10.3390/en11071749.

[11] J. Teh and C.-M. Lai, "Reliability impacts of the dynamic thermal rating and battery energy storage systems on wind-integrated power networks," *Sustain. Energy Grids Netw.*, vol. 20, p. 100268, Dec. 2019, doi: 10.1016/j.segan.2019.100268.

[12] J. Teh, "Adequacy Assessment of Wind Integrated Generating Systems Incorporating Demand Response and Battery Energy Storage System," *Energies*, vol. 11, no. 10, 2018, doi: 10.3390/en11102649.

[13] M. K. Metwaly and J. Teh, "Probabilistic Peak Demand Matching by Battery Energy Storage Alongside Dynamic Thermal Ratings and Demand Response for Enhanced Network Reliability," *IEEE Access*, vol. 8, pp. 181547–181559, 2020, doi: 10.1109/ACCESS.2020.3024846.

[14] H. Jabir, J. Teh, D. Ishak, and H. Abunima, "Impacts of Demand-Side Management on Electrical Power Systems: A Review," *Energies*, vol. 11, no. 5, 2018, doi: 10.3390/en11051050.

[15] J. Teh, C. A. Ooi, Y. H. Cheng, M. Zainuri, and C. M. Lai, "Composite Reliability Evaluation of Load Demand Side Management and Dynamic Thermal Rating Systems," *Energies*, vol. 11, no. 2, 2018, doi: 10.3390/en11020466.

[16] W. C. Khoo, J. Teh, and C. -M. Lai, "Demand Response and Dynamic Line Ratings for Optimum Power Network Reliability and Ageing," *IEEE Access*, vol. 8, pp. 175319–175328, 2020, doi: 10.1109/ACCESS.2020.3026049.

[17] H. Jabir, J. Teh, D. Ishak, and H. Abunima, "Impact of Demand-Side Management on the Reliability of Generation Systems," *Energies*, vol. 11, no. 8, 2018, doi: 10.3390/en11082155.

[18] H. Abunima, J. Teh, C.-M. Lai, and H. Jabir, "A Systematic Review of Reliability Studies on Composite Power Systems: A Coherent Taxonomy Motivations, Open Challenges, Recommendations, and New Research Directions," *Energies*, vol. 11, no. 9, 2018, doi: 10.3390/en11092417.

[19] P. M. Anderson and B. K. LeReverend, "Industry experience with special protection schemes," *IEEE Trans. Power Syst.*, vol. 11, no. 3, pp. 1166–1179, 1996, doi: 10.1109/59.535588.

[20] B. Jimada-Ojuolape and J. Teh, "Impact of the Integration of Information and Communication Technology on Power System Reliability: A Review," *IEEE Access*, vol. 8, pp. 24600–24615, 2020, doi: 10.1109/access.2020.2970598.

[21] B. Jimada-Ojuolape and J. Teh, "Surveys on the reliability impacts of power system cyber–physical layers," *Sustain. Cities Soc.*, vol. 62, p. 102384, Nov. 2020, doi: 10.1016/j.scs.2020.102384.

[22] J. Teh and C. Lai, "Reliability Impacts of the Dynamic Thermal Rating System on Smart Grids Considering Wireless Communications," *IEEE Access*, vol. 7, pp. 41625–41635, 2019, doi: 10.1109/access.2019.2907980.

[23] V. Madani *et al.*, "IEEE PSRC Report on Global Industry Experiences With System Integrity Protection Schemes (SIPS)," *IEEE Trans. Power Deliv.*, vol. 25, no. 4, pp. 2143–2155, 2010, doi: 10.1109/TPWRD.2010.2046917.

[24] S. H. Ghanam, B. S. Shahrani, A. S. Essa, M. M. Hamrani, F. A. Dubaikel, and A. T. Awami, "Saudi ARAMCO's efforts in smart grid," in *2011 IEEE PES Conference on Innovative Smart Grid Technologies - Middle East*, Dec. 2011, pp. 1–9, doi: 10.1109/ISGT-MidEast.2011.6220797.

[25] J. Teh and C. Lai, "Risk-Based Management of Transmission Lines Enhanced With the Dynamic Thermal Rating System," *IEEE Access*, vol. 7, pp. 76562–76572, 2019, doi: 10.1109/access.2019.2921575.

[26] "IEEE Standard for Calculating the Current-Temperature of Bare Overhead Conductors," *IEEE Std 738-2006 Revis. IEEE Std 738-1993*, pp. c1-59, 2007, doi: 10.1109/IEEESTD.2007.301349.

[27] J. Teh *et al.*, "Prospects of Using the Dynamic Thermal Rating System for Reliable Electrical Networks: A Review," *IEEE Access*, vol. 6, pp. 26765–26778, 2018, doi: 10.1109/access.2018.2824238.

[28] J. Teh and I. Cotton, "Risk informed design modification of dynamic thermal rating system," *IET Gener. Transm. Distrib.*, vol. 9, no. 16, pp. 2697–2704, 2015, doi: 10.1049/iet-gtd.2015.0351.

[29] J. Teh and I. Cotton, "Reliability Impact of Dynamic Thermal Rating System in Wind Power Integrated Network," *IEEE Trans. Reliab.*, vol. 65, no. 2, no. 2, pp. 1081–1089, Jun. 2016, doi: 10.1109/tr.2015.2495173.

[30] J. Teh and I. Cotton, "Critical span identification model for dynamic thermal rating system placement," *IET Gener. Transm. Distrib.*, vol. 9, no. 16, pp. 2644–2652, 2015, doi: 10.1049/iet-gtd.2015.0601.

[31] J. Wang, X. Xiong, J. Hu, and X. Lu, "Safety strategy of power transmission channel coordinated with transfer capability support for power system emergency," *Int. J. Electr. Power Energy Syst.*, vol. 110, pp. 232–245, Sep. 2019, doi: 10.1016/j.ijepes.2019.03.017.

[32] J. Hu, X. Xiong, and J. Wang, "Current Tolerance Capability Calculation Model of Transmission Lines and its Application in Overload Protection," *Electr. Power Compon. Syst.*, vol. 46, no. 14–15, pp. 1509–1521, Sep. 2018, doi: 10.1080/15325008.2018.1511005.

[33] A. Piccolo, A. Vaccaro, and D. Villacci, "Thermal rating assessment of overhead lines by Affine Arithmetic," *Electr. Power Syst. Res.*, vol. 71, no. 3, pp. 275–283, Nov. 2004, doi: 10.1016/j.epsr.2004.01.018.

[34] H. Shaker, M. Fotuhi-Firuzabad, and F. Aminifar, "Fuzzy Dynamic Thermal Rating of Transmission Lines," *IEEE Trans. Power Deliv.*, vol. 27, no. 4, pp. 1885–1892, 2012, doi: 10.1109/TPWRD.2012.2193672.

[35] J. Teh, "Uncertainty Analysis of Transmission Line End-of-Life Failure Model for Bulk Electric System Reliability Studies," *IEEE Trans. Reliab.*, vol. 67, no. 3, pp. 1261–1268, 2018, doi: 10.1109/tr.2018.2837114.

[36] K. R. W. Bell, A. R. Daniels, and R. W. Dunn, "Alleviation of transmission system overloads using fuzzy reasoning," *Appl. Fuzzy Theory Electron. Power Syst.*, vol. 102, no. 1, pp. 41–52, Feb. 1999, doi: 10.1016/S0165-0114(97)00201-7.

[37] A. k. Deb, *Power Line Ampacity System -- Theory, Modelling and Applications*. Boca Raton, FL: CRC, 2000.

[38] Y. Zhang, Y. Xu, and Z. Y. Dong, "Robust Ensemble Data Analytics for Incomplete PMU Measurements-Based Power System Stability Assessment," *IEEE Trans. Power Syst.*, vol. 33, no. 1, pp. 1124–1126, Jan. 2018, doi: 10.1109/TPWRS.2017.2698239.

[39] L. G. Meegahapola, S. Bu, D. P. Wadduwage, C. Y. Chung, and X. Yu, "Review on Oscillatory Stability in Power Grids With Renewable Energy Sources: Monitoring, Analysis, and Control Using Synchrophasor Technology," *IEEE Trans. Ind. Electron.*, vol. 68, no. 1, pp. 519–531, Jan. 2021, doi: 10.1109/TIE.2020.2965455.

[40] W. Z. Black and R. L. Rehberg, "Simplified Model for Steady State and Real-Time Ampacity of Overhead Conductors," *IEEE Trans. Power Appar. Syst.*, vol. PAS-104, no. 10, pp. 2942–2953, Oct. 1985, doi: 10.1109/TPAS.1985.319142.

[41] "IEEE Standard for Synchrophasor Data Transfer for Power Systems," *IEEE Std C371182-2011 Revis. IEEE Std C37118-2005*, pp. 1–53, Dec. 2011, doi: 10.1109/IEEESTD.2011.6111222.

[42] K. A and G. Madan M, *Introduction to Fuzzy Arithmetic Theory and Application*. New York: Van Nostrand Reinhold Co., 1991.

[43] S. Abbasbandy and T. Hajjari, "A new approach for ranking of trapezoidal fuzzy numbers," *Comput. Math. Appl.*, vol. 57, no. 3, pp. 413–419, Feb. 2009, doi: 10.1016/j.camwa.2008.10.090.

[44] C.-H. Cheng, "A new approach for ranking fuzzy numbers by distance method," *Fuzzy Sets Syst.*, vol. 95, no. 3, pp. 307–317, May 1998, doi: 10.1016/S0165-0114(96)00272-2.

[45] M. Ma, A. Kandel, and M. Friedman, "A new approach for defuzzification," *Fuzzy Sets Syst.*, vol. 111, no. 3, pp. 351–356, May 2000, doi: 10.1016/S0165-0114(98)00176-6.

[46] M. Jiménez, M. Arenas, A. Bilbao, and M. V. Rodrı´guez, "Linear programming with fuzzy parameters: An interactive method resolution," *Eur. J. Oper. Res.*, vol. 177, no. 3, pp. 1599–1609, Mar. 2007, doi: 10.1016/j.ejor.2005.10.002.

[47] "Kingdom of Saudi Arabia open data portal." [Online]. Available: https://data.gov.sa/en/home.

Mohamed K. Metwaly received the B.Sc (first class honors). and M.Sc. degrees in Electrical Engineering from Menoufia University, Shebin El-Kom, Egypt, in 1999, and 2003, respectively, and the Ph.D. degree in electrical engineering (with distinction) from Vienna University of Technology, Vienna, Austria, in 2009. In 2000, he became an Instructor with the Department of Electrical Engineering, Faculty of Engineering; Menoufia University, and then was an Assistant Lecturer in 2003. From 2010 to 2015, he became lecturer with the Department of Electrical Engineering, Faculty of Engineering; Menoufia University, where he became an Assistant Professor, from 2015 to 2020. In June 2020, he promoted with scientific excellence to Professor in the field control of electric machines with the Department of Electrical Engineering, Faculty of Engineering, Menoufia University. His research interests include control of ac machines, applications of power electronics, power factor correction converters, sensorless control of electric drives, renewable energy applications, stability analysis of control systems; observers and estimators, and digital signals processing based real-time control.

Jiashen Teh received the B.Eng (first class honors) in electrical and electronic engineering from Universiti Tenaga Nasional (UNITEN), Selangor, Malaysia, in 2010 and the Ph.D degree in similar field from the University of Manchester, Manchester, UK, in 2016.

Since 2016, he is a Senior Lecturer/Assistant Professor at the Universiti Sains Malaysia (USM), Penang, Malaysia. In 2018, he was appointed and served as an Adjunct Professor at the Green Energy Electronic Center of National Taipei University of Technology (Taipei Tech), Taipei, Taiwan. Since 2019, he has been an Adjunct Professor at the Intelligent Electric Vehicle & Green Energy Center of National Chung Hsing University (NCHU), Taichung, Taiwan. His research interests include probabilistic modelling of power systems, grid-integration of renewable energy sources and reliability modelling of smart grid networks.

Dr. Teh is a Chartered Engineer (CEng) conferred by the Engineering Council, UK, and The Institution of Engineering and Technology (IET), a registered Professional Engineer (P.Eng) with the Board of Engineers Malaysia (BEM), a member of IEEE Power and Energy Society and the Institution of Engineers Malaysia (IEM). He received the outstanding publication awards from USM in from 2016 to 2019. He is also a regular invited reviewer for International Journal of Electrical Power and Energy Systems, IEEE Access, IEEE Transactions on Industry Applications, IEEE Transactions on Vehicular Technology, IEEE Transactions on Reliability, IEEE Transactions on Industrial Electronics, and The IET Generation, Transmission and Distribution.